Physics Letters A 432 (2022) 128010

Contents lists available at ScienceDirect

Physics Letters A

www.elsevier.com/locate/pla

Theoretical study of magnetic phase transition in $La_{\frac{2}{3}}M_{\frac{1}{3}}MnO_3$ (M=Ca, Sr) membranes through strain and doping

Jia-Yi Lin, Zhong-Jia Chen, Guan-Liang Li, Jiarui Zeng, Yu-Jie Cen, Wen-Qiang Xie, Yin-Hui Peng, Ji-Hai Liao, Xiao-Bao Yang, Yu-Jun Zhao *

Department of Physics, South China University of Technology, Guangzhou, 510640, People's Republic of China

ARTICLE INFO

Article history:
Received 7 October 2021
Received in revised form 23 January 2022
Accepted 14 February 2022
Available online 18 February 2022
Communicated by L.M. Woods

Keywords:
$La_{\frac{2}{3}}M_{\frac{1}{3}}MnO_3$ (M=Ca, Sr)
Magnetic phase transition
Strain
Charge doping
First-principles calculation

ABSTRACT

The antiferromagnetic-semiconductor extreme tensile strain (8%) states of $La_{0.7}Ca_{0.3}MnO_3$ membranes was achieved by Hong *et al.* (2020) [23]. To understand such tunable magnetic and electronic properties in these $La_{\frac{2}{3}}M_{\frac{1}{3}}MnO_3$ (M=Ca, Sr) systems, we have investigated the magnetic and electronic behaviors of $La_{\frac{2}{3}}M_{\frac{1}{3}}MnO_3$ (M=Ca, Sr) under strain and charge doping using first-principles calculations. A ferromagnetic-semiconductor phase is predicted for $La_{\frac{2}{3}}Sr_{\frac{1}{3}}MnO_3$ beyond 4% biaxial tensile strain. Meanwhile, its energy gap and magnetic anisotropic energy increase as the strain increases. We also discover that the change of magnetic exchange energy in $La_{\frac{2}{3}}Ca_{\frac{1}{3}}MnO_3$ under charge doping is in analogy to the scenario directly changing the Ca concentrations. Based on the magnetic competition analysis, it is expected that the carrier concentration and strains dominate the magnetic ground state while the La/Ca distributions have little impact. The highly tunable magnetic-electronic properties offer opportunities for the future magnetic-electronic materials design and applications.

1. Introduction

Over the last several decades, great efforts have been devoted to the research of $La_{1-x}M_xMnO_3$ (M = Ca, Sr) and the relevant compounds, due to their metal–insulator transition [1]. Manganites with such general formula are perovskite structures, displaying various interesting phenomena, such as large magnetocaloric effect [2], high-temperature superconductivity [3,4], and the colossal magnetoresistence [5–7]. Such novel properties extremely rely on the doping concentration x as well as external conditions, such as strain, pressure, temperature, electric or magnetic field. As typical strongly correlated electron systems, rare-earth perovskite manganites have multiple phases which are coupled to the lattice [8]. As a result, quite a number of stable and meta-stable magnetic and electronic states arise at different strain and carrier concentrations, indicating that such materials are promising in the future device applications.

Experimental study on these manganite oxides have been the subject of intense research. Particularly, the $La_{1-x}M_xMnO_3$ series, with M = Ca, Sr, undergo a phase transition from a high-temperature paramagnetic insulating phase to a low-temperature ferromagnetic half-metallic phase in the range of $0.2 < x < 0.5$ [9]. The maximal Curie temperature T_c is around 250 K for $La_{1-x}Ca_xMnO_3$ and 370 K for $La_{1-x}Sr_xMnO_3$ around $x = \frac{1}{3}$ [10,11], in which charge-ordered states [12], and large magnetocaloric effect [13–16] were also observed experimentally. The half-metallic ground state of these materials is closely adjacent to many other phases which are coupled to the lattice, offering an excellent platform to understand electronic correlation physics dominated by lattice strain [17,18]. Although the ultrathin membranes of these materials have been prepared in experiments for years [19–21], the extreme tensile strain states had not been achieved experimentally for a very long time in bulk oxides. Those crystals are usually so brittle that suffer from cracking under relatively small tensile strain. It was believed that a slightly larger strain state in such complex oxide materials may only access via compressive strain [22]. In 2020, Hong *et al.* [23] firstly realized the extreme tensile strain states mechanically in $La_{0.7}Ca_{0.3}MnO_3$ ultrathin films exceeding 8% uniaxially as well as 5% biaxially in their experiment, shedding a light on the possibilities of the extreme strain engineering of a series of analogous complex oxide membrane materials. In the same year, McLeod *et al.* [24] achieved the multi-messenger nanoprobes of hidden magnetism in slightly strained $La_{\frac{2}{3}}Ca_{\frac{1}{3}}MnO_3$ films, guiding futural functional engineering of similar magnetic oxides into the regime of phase-programmable

* Corresponding author.
E-mail address: zhaoyj@scut.edu.cn (Y.-J. Zhao).

https://doi.org/10.1016/j.physleta.2022.128010
0375-9601/

materials. As is well known, charge doping is another effective way to control the magnetic and electronic properties of magnetic materials [25–28]. However, to our knowledge, such experiments have not been demonstrated in these manganite films yet.

The theoretical pioneer to explain the electronic and magnetic behaviors of these mixed-valency manganites was the double-exchange model proposed by Zener and the Heisenberg model [29–31]. They did qualitatively describe the magnetic and electronic properties of these manganites but remarkably overestimated the Curie temperature [32,33]. Other theoretical studies of these series were performed using first-principles calculations. Early tries mostly focused on the end compound $LaMnO_3$. However, no matter using the density-functional theory (DFT), or the Hartree-Fock (HF) method, the antiferromagnetic ground state and band structure were not described correctly [34–39]. Such ambiguities originate from the well-kown nature that the DFT method is hard to describe the exchange of electrons precisely while the HF method ignores the correlation energy [40,41]. In 2005, Trimarchi *et al.* [42] tackled the system via the DFT+U method. Their work, however, was based on ultrasoft pseudopotentials, which were believed to be less accurate in magnetic properties than other state-of-the-art pseudopotentials [43]. Fortunately, Korotana *et al.* [44,45] successfully described the properties of the end compounds and $La_{0.75}Ca_{0.25}MnO_3$ using Becke three-parameter Lee-Yang-Parr (B3LYP) hybrid-exchange DFT calculations. However, hybrid-exchange DFT calculations cost so heavily that it is unaffordable now for many other doping concentrations because significantly larger supercells are necessary for such simulations. Other calculations to solve different problems about this series were also carried out with different methods [46–50]. Generally speaking, meta-GGA functionals are expected to have a better overall performance than GGA or LDA functionals, however, such calculation results about $La_{1-x}M_xMnO_3$ have not been reported yet. Furthermore, few theoretical discussions are available about the variable magnetic and electronic properties of compressive strain states of $La_{\frac{2}{3}}Ca_{\frac{1}{3}}MnO_3$, the extreme tensile and compressive strain states of $La_{\frac{2}{3}}Sr_{\frac{1}{3}}MnO_3$, and the charge doping states of the both series. In consideration of the significant progress of the extreme tensile strain experiment of $La_{0.7}Ca_{0.3}MnO_3$, a comprehensive theoretical study about these problems is significantly desired at present.

In this work, we report a systematic theoretical study of $La_{\frac{2}{3}}M_{\frac{1}{3}}MnO_3$, with M = Ca, Sr, under different strains and charge doping conditions using DFT+U calculation with strongly constrained and appropriately normed (SCAN) functional [51,52], which is expected to be more accurate than most semilocal functionals [53]. Interestingly, we computationally discover that the magnetic behaviors of charge doped $La_{\frac{2}{3}}Ca_{\frac{1}{3}}MnO_3$ is similar to the directly changing of the Ca doping concentration x. Furthermore, $La_{\frac{2}{3}}Sr_{\frac{1}{3}}MnO_3$ will turn into a ferromagnetic-semiconductor ground state when biaxially strained exceeding 4%. Meanwhile, the energy gap as well as the magnetic anisotropic energy is enlarged as the strain is introduced.

2. Computational details

All our calculations are conducted using DFT. The projector-augmented wave (PAW) approach was used [54], performed in the Vienna *ab initio* simulation package (VASP) [55–57]. The computations were done within the meta-generalized gradient approximation (meta-GGA) with SCAN functional to describe the exchange and correlation energy. The energy cutoff was set to 560 eV for the plane wave basis set to expand the Kohn-Sham wavefunction [58,59]. The total energy of $La_{2/3}Sr_{1/3}MnO_3$ is converged to within 0.1 meV/atom as the cutoff energy increases from 480 eV to 600 eV. The criterion for energy convergence of the electronic self-consistent calculation was no more than 5×10^{-6} eV/cell. All the coordinations of the atoms were fully relaxed until the residual forces on each atom were smaller than 0.01 eV/Å. In order to appropriately include the strong electrons correlations of the d and f electrons, we adopted the DFT+U method with the interaction parameters of U(Mn,3d) = 3.9 eV, J(Mn,3d) = 0.9 eV for $La_{\frac{2}{3}}Ca_{\frac{1}{3}}MnO_3$ while U(Mn,3d) = 3.4 eV, J(Mn,3d) = 0.9 eV for $La_{\frac{2}{3}}Sr_{\frac{1}{3}}MnO_3$ and U(La,4f) = 6 eV, J(La,4f) = 1 eV for both. These U and J values give reasonable lattice parameters and correct antiferromagnetic ground state of $LaMnO_3$. 8×8×2 and 8×8×4 Γ-centered Monkhorst-Pack k-point meshes for $La_{\frac{2}{3}}Ca_{\frac{1}{3}}MnO_3$ and $La_{\frac{2}{3}}Sr_{\frac{1}{3}}MnO_3$ were employed, respectively. We used the following electronic configurations: $5s^25p^65d^16s^2$ for La, $3s^23p^64s^2$ for Ca, $4s^24p^65s^2$ for Sr, $3s^23p^63d^54s^2$ for Mn, and $2s^22p^4$ for O. The semi-core electrons of Mn, Ca and Sr were included in our calculations in order to get a more accurate description. The search of equivalent crystal structure and data post-processing were done by SAGAR code and the vaspkit program [60–62].

3. Results and discussion

3.1. Structures of $La_{\frac{2}{3}}Ca_{\frac{1}{3}}MnO_3$ and $La_{\frac{2}{3}}Sr_{\frac{1}{3}}MnO_3$

Both $La_{\frac{2}{3}}Ca_{\frac{1}{3}}MnO_3$ and $La_{\frac{2}{3}}Sr_{\frac{1}{3}}MnO_3$ are of the nature of a solid-solution configuration [10,11,23]. If the La and Ca/Sr ions are not distinguished, the $La_{\frac{2}{3}}Ca_{\frac{1}{3}}MnO_3$ structure is an orthorhombic perovskite crystal structure with a *Pnma* space group [10]. As for the $La_{\frac{2}{3}}Sr_{\frac{1}{3}}MnO_3$, a rhombohedral perovskite structure with a $R\bar{3}c$ space group is observed [11]. Here, we will not focus on the solid-solution configuration. Instead, the ordered distributions were employed. Actually, Hong *et al.* [23] have tested the influence of the La/Ca distributions in their work and the configuration impact to the magnetic transitions are not remarkable in their results. For the $La_{\frac{2}{3}}Ca_{\frac{1}{3}}MnO_3$, we build a most symmetrical 1×1×3 supercell from the *Pnma* $LaMnO_3$. After full structural relaxation for each of the possible configurations in the FM ordering, the most energetically favorable one is selected for further investigation from the 32 configurations. As for the $La_{\frac{2}{3}}Sr_{\frac{1}{3}}MnO_3$, the minimal cell necessary for the calculation of this doping concentration x is the $R\bar{3}c$ $LaMnO_3$ primitive cell and there are only 3 nonequivalent configurations of the distributions. We also choose the most energetically favorable configuration for the following studies. Both of them have the highest symmetry among these distributions. The fully relaxed lattice parameters are listed in Table 1 for $La_{\frac{2}{3}}Ca_{\frac{1}{3}}MnO_3$ and $La_{\frac{2}{3}}Sr_{\frac{1}{3}}MnO_3$. These parameters are in excellent agreement with the experimental results [10,11]. In both structures, Mn ions are located in the MnO_6 octahedra cages, which are tilted and distorted by different Mn-O bond lengths due to the Jahn-Teller distortion [63]. The structures of $La_{\frac{2}{3}}Ca_{\frac{1}{3}}MnO_3$, $La_{\frac{2}{3}}Sr_{\frac{1}{3}}MnO_3$ and the corresponding Jahn-Teller distorted structure of MnO_6 octahedra are shown in Fig. 1(a)-(c).

3.2. The biaxial and compressive strain of $La_{\frac{2}{3}}Ca_{\frac{1}{3}}MnO_3$

In $La_{1-x}Ca_xMnO_3$ series, there are 4 different stable magnetic states in different Ca concentration x, namely the A-, C-, G-type antiferromagnetic states and the ferromagnetic state [64]. The four types spin configurations are shown in Fig. 2. Generally speaking, the magnetic competition mechanism in $La_{1-x}Ca_xMnO_3$ compounds is accepted as following: the Mn^{3+}-O-Mn^{4+} double exchange supports the ferromagnetic order while the Jahn-Teller distortion benefits the formation of A-type antiferromagnetic order

Table 1
The calculated and experimental lattice parameters of $La_{\frac{2}{3}}M_{\frac{1}{3}}MnO_3$ (M = Ca, Sr).

$La_{\frac{2}{3}}Ca_{\frac{1}{3}}MnO_3$	a (Å)	b (Å)	c (Å)	α (deg)	β (deg)	γ (deg)	Ref
Theo. values	5.4585	5.4715	7.7085	90	90	90	
Expt. values	5.4515	5.4671	7.7004	90	90	90	[10]
$La_{\frac{2}{3}}Sr_{\frac{1}{3}}MnO_3$							
Theo. values	5.4976	5.4976	13.3525	90	90	120	
Expt. values	5.5073	5.5073	13.3626	90	90	120	[11]

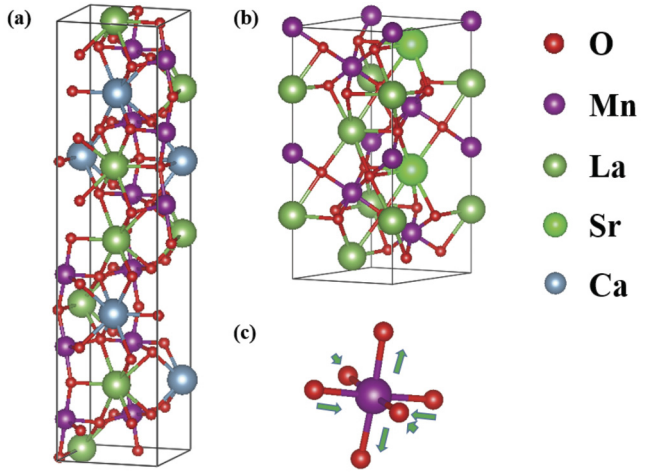

Fig. 1. Structures of $La_{\frac{2}{3}}M_{\frac{1}{3}}MnO_3$. The purple, red, bottle green, blue, jade-green balls correspond to the Mn, O, La, Ca, Sr atoms, respectively. Crystallographic cells used in calculations for (a) $La_{\frac{2}{3}}Ca_{\frac{1}{3}}MnO_3$, (b) $La_{\frac{2}{3}}Sr_{\frac{1}{3}}MnO_3$. (c) The Jahn-Teller distorted structure of MnO_6 octahedra. (For interpretation of the colors in the figure(s), the reader is referred to the web version of this article.)

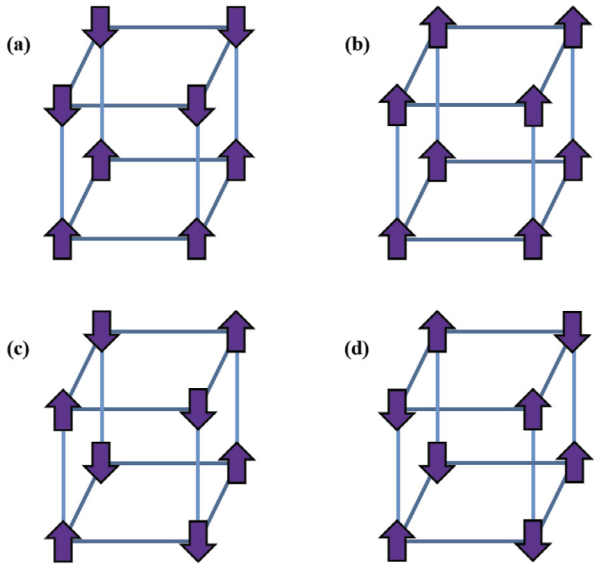

Fig. 2. The magnetic configurations in $La_{1-x}Ca_xMnO_3$ with the local magnetic moments of Mn are represented by the arrows. (a) A-type antiferromagnetic (A-AFM) order; (b) Ferromagnetic (FM) order; (c) C-type antiferromagnetic (C-AFM) order; (d) G-type antiferromagnetic (G-AFM) order.

[44], and the Mn^{4+}-O-Mn^{4+} superexchange give rise to the G-type antiferromagnetic order [65].

We have first calculated the structural, magnetic and electronic properties of $La_{\frac{2}{3}}Ca_{\frac{1}{3}}MnO_3$ with no ambient strain or charge doping. In our calculation, not only the lattice parameters have no remarkable difference from the experimental values as listed in Table 1, but also the average magnetic moment (3.67 μ_B/Mn) is in line with the experimental value of 3.5 μ_B/Mn very well [66]. The ground state of the experimental ferromagnetic half-metal phase is reproduced, as shown in Fig. 3(a). Meanwhile, the calculated energy difference between A-AFM and FM states is about 44 meV per formula unit (f.u.), agreeing well with the experimental result [23]. Such energy difference is greater than the energy scale kT of room-temperature and the numerical error of the DFT calculations. We did not conduct the SCF calculations with SOC since its influence on magnetic exchange energy is typically no more than 1 meV/magnetic-atom [67]. We also carefully tested the influence of SOC on the magnetic exchange energy with the $LaMnO_3$ primitive cell to ensure that the SOC effect will not change our conclusion. All the above validates the reliability of our calculations. To simulate the behaviors of the materials under strain conditions, we artificially enlarge values of a, b lattice parameters then relaxed c axis for biaxial tensile strain while reducing the c lattice parameter and relaxing the a, b axes for compressive strain. In our simulation, $La_{\frac{2}{3}}Ca_{\frac{1}{3}}MnO_3$ undergoes a transition from an FM half-metal ground state to A-AFM semiconductor ground state when biaxially strained exceeding 4% as shown in Fig. 3(b)(d), in line with the result from Hong *et al.* [23]. Similar results are obtained when the c axis is compressed by 4% as shown in Fig. 3(c)(e). It is widely accepted that the FM state in $La_{1-x}Ca_xMnO_3$ is originated from the double exchange of Mn-O-Mn [29,30]. The Jahn-Teller distortion will suppress the double exchange and give rise to an A-AFM configuration. Here, we take the bond length difference between the longest and shortest ones/average-bond-length*100% as an indicator to measure the Jahn-Teller distortion. Such bond length difference increases from about 3.6% (no strain) to 20.48% (biaxial strain of 8%). Experimentally, isotropic pressure can suppress the Jahn-Teller distortion, and subsequently enhance the ferromagnetism and Curie temperature of $La_{0.7}M_{0.3}MnO_3$ (M=Ca, Sr) [10,11]. Strains will enlarge the difference of the Mn-O bond length in a MnO_6 octahedra, enhancing the Jahn-Teller effect [23]. Therefore, we expect that the transition of $La_{\frac{2}{3}}Ca_{\frac{1}{3}}MnO_3$ from an FM half-metal ground state to the A-AFM semiconductor ground state roots from the enhancement of Jahn-Teller distortion. Particularly, we discover that the energy of C-AFM, G-AFM states considerably decrease with respect to that of FM state as the strain increases. This means that the exchange energy will descend fast when the lattice is distorted. We also fit the equation of state following Murnaghan formalism [68] as shown in Fig. 3(f). Of note, the volume of the system may not be the same for a given value of c during c-compressive strain and a-b tensile strain due to the kinetic barrier during the relaxation.

To further explore the atomic size effect on above magnetic behaviors, we directly replaced the Ca atoms by Sr atoms in the optimized $La_{\frac{2}{3}}Ca_{\frac{1}{3}}MnO_3$ structures under different strain conditions then performed electronic self-consistent calculations with different magnetic orders. In our computations, all the energy difference of AFM and FM states change merely about 2 meV. This indicates that the atomic size effect has little influence. Instead, the carrier concentration combined with the Jahn-Teller distortion dominate the magnetic exchange energy in this series from our following demonstration.

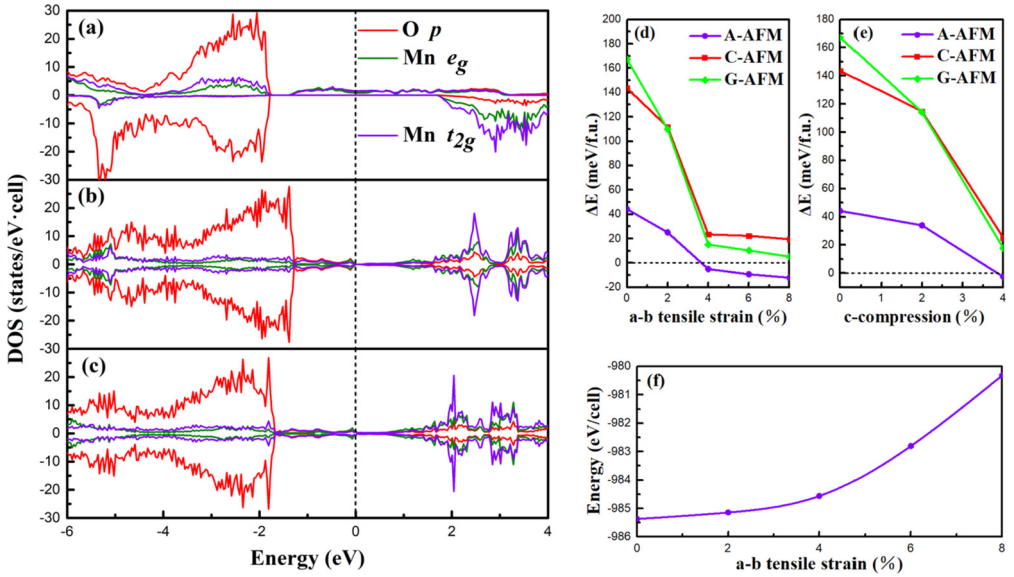

Fig. 3. Strain effect on the density of states and energy of $La_{\frac{2}{3}}Ca_{\frac{1}{3}}MnO_3$. (a) The PDOS of $La_{\frac{2}{3}}Ca_{\frac{1}{3}}MnO_3$ without strain. **(b)** The PDOS of biaxial strain 4% state. (c) The PDOS of compressive strain 4% state along *c* axis. (d) E_{AFM}-E_{FM} vs. biaxial strain. (e) E_{AFM}-E_{FM} for compressive strain states along *c* axis. (f) The energy for various biaxial strain states.

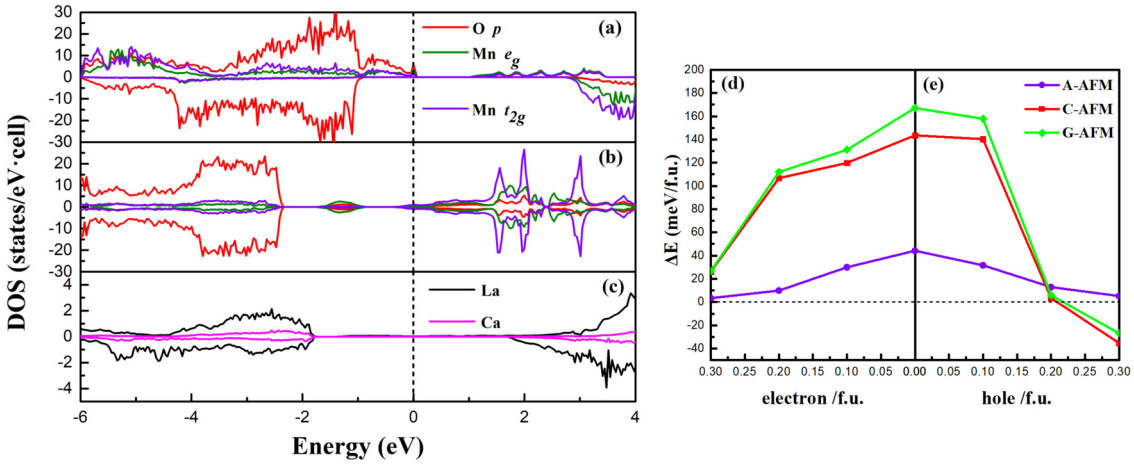

Fig. 4. Charge doping of $La_{\frac{2}{3}}Ca_{\frac{1}{3}}MnO_3$. (a) The PDOS of doped 0.3 electron/f.u. state. **(b)** The PDOS of doped 0.3 hole/f.u. state. (c) The PDOS of La and Ca ions with no ambient conditions. (d) E_{AFM}-E_{FM} vs. electron doping. (e) E_{AFM}-E_{FM} vs. hole doping.

3.3. The charge doped $La_{\frac{2}{3}}Ca_{\frac{1}{3}}MnO_3$

Consequently, we evaluate the effect of both electron doping and hole doping in $La_{\frac{2}{3}}Ca_{\frac{1}{3}}MnO_3$. In our calculations, $La_{\frac{2}{3}}Ca_{\frac{1}{3}}MnO_3$ undergoes a phase transition from FM to C-AFM ground state when hole doping concentration reaches 0.3 hole/f.u. as shown in Fig. 4(e). As for electron doping, although no magnetic-electronic phase transition takes place in our simulation, the energy difference between FM and A-AFM state is only about 3 meV at doping concentration of 0.3 electron/f.u. as shown in Fig. 4(d). At the same time, the exchange energy reduction also accelerates as the charge doping enhances. It is worth to note that the performance of the magnetic ground states vs. charge doping is quite analogous to the scenario of directly changing the Ca doping concentration. For comparison, $La_{1-x}Ca_xMnO_3$ is in C-AFM ground state when x = 0.6 while in A-AFM ground state when x = 0 [64]. To explore the origin of such phenomenon, we have plotted the PDOS of the valence electrons of La and Ca ions, as shown in Fig. 4(c). It is obvious that the energy levels of these orbitals are relatively far away from the Fermi level. Thus, we suggest that the Ca doping mainly affects the carrier concentration in $La_{1-x}Ca_xMnO_3$, dominating the magnetic exchanges of Mn ions and the extent of Jahn-Teller distortion. As a result, the magnetic ground state is determined. Furthermore, the magnetic exchanges of Mn 3*d* electrons are mediated by O 2*p* orbitals while the La/Ca ions do not directly participate in such exchanges. So it is expected that the distributions of La/Ca barely influence the magnetic ground state of $La_{1-x}Ca_xMnO_3$ series. As a comparison, Hong *et al.* [23] calculated energy differences of FM and A-AFM states of strained $La_{0.69}Ca_{0.31}MnO_3$ as well as $La_{0.75}Ca_{0.25}MnO_3$ with random La/Ca distributions. They reported that all the structures favor A-AFM ground state near the experimental critical points due to the enhanced Jahn-Teller distortion under strain. Here, we suppose that the carrier concentration combined with external conditions such as strain and pressure, dominate the magnetic ground state as well as the exchange energy while the La/Ca distributions have little impact on the magnetic properties of $La_{1-x}Ca_xMnO_3$. This explains why this series is of the nature of solid-solution but the magnetic ground state is not sensitive to the La/Ca distributions. Meanwhile, the Curie temperature T_c is also in a very small range at specific Ca concentration x in a number of different experiments [10,11].

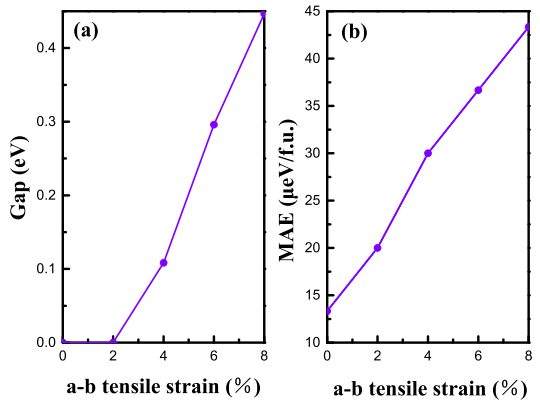

Fig. 5. The gap and MAE of $La_{\frac{2}{3}}Sr_{\frac{1}{3}}MnO_3$ as strain applied. **(a)** The gap of $La_{\frac{2}{3}}Sr_{\frac{1}{3}}MnO_3$. **(b)** The MAE of $La_{\frac{2}{3}}Sr_{\frac{1}{3}}MnO_3$.

3.4. The case of $La_{\frac{2}{3}}Sr_{\frac{1}{3}}MnO_3$

As for the case of $La_{\frac{2}{3}}Sr_{\frac{1}{3}}MnO_3$, we also obtained an average magnetic moment of 3.67 μ_B/Mn when no ambient condition is imposed, in line with the experimental value of 3.7 μ_B/Mn very well [69]. The calculated spin-down band gap is about 3 eV as shown in Fig. 6(a), close to the experimental values [48]. In order to understand the magnetic behaviors of this material, we have identified all the nonequivalent Mn ions via self-developed SAGAR codes then calculated the energy difference between FM and all possible AFM states with various strains. Interestingly, as shown in Fig. 6(b)(c)(f), contrast to the $La_{\frac{2}{3}}Ca_{\frac{1}{3}}MnO_3$ case, $La_{\frac{2}{3}}Sr_{\frac{1}{3}}MnO_3$ never favors the AFM ground state but becomes ferromagnetic-semiconductor ground state as the biaxial strain is imposed exceeding 4%. At the same time, the band gap is enlarged as the biaxial strain is performed as Fig. 5(a) shown. Furthermore, all the energy difference between FM and AFM states reaches a plateau in the range of about 20 meV after becoming ferromagnetic-semiconductor ground state structures. This suggests that the ferromagnetic-semiconductor ground state is robust in such process. Similar phenomenon also emerged in $LaMnO_3$ related superlattice [70]. Moreover, we also calculated the magnetic anisotropic energy (MAE) by arranging all the magnetic moments along *x*, *y*, *z* axes, respectively, with spin-orbit coupling (SOC) included. To our knowledge, the SOC effect has been discussed in $LaMnO_3$ end compound [71] but has not been investigated in the doped series. From our calculations, we find that the *z* direction magnetization is most energetic favored while the *x* and *y* magnetization have the same energy. So it seems that the *c* axis is close to the easy axis in $La_{\frac{2}{3}}Sr_{\frac{1}{3}}MnO_3$ films. It is worth to note that the MAE would be enhanced as biaxial strain is applied, from 13.33 μeV without strain to 43.33 μeV with 8% biaxial strain as shown in Fig. 5(b). Such MAE values are much more greater than numbers of well-known room-temperature magnetic element crystals, such as iron, cobalt and nickel, of which the MAE is typically on the order of 1 μeV [72]. Generally, ideal candidate for spin field-effect transistor needs to be ferromagnetic semiconductor with high MAE, which is believed to be rare [73].

In the case of compressive strain states of $La_{\frac{2}{3}}Sr_{\frac{1}{3}}MnO_3$, we predict that it will undergo a phase transition from an FM-metallic state to a ferrimagnetic (FerriM)-semiconductor state when the *c* lattice parameter is compressed beyond 10% as shown in Figs. 6(d)(f). Various initial AFM magnetic configurations always converge to FerriM states after relaxation. Typically, the dominant magnetic coupling are the nearest and next nearest coupling while the longer range interactions contribute little to the magnetic exchange energy [25]. Via SAGAR codes, we have tried 6 initial AFM configurations of $La_{\frac{2}{3}}Sr_{\frac{1}{3}}MnO_3$ with its *c* lattice parameter compressed beyond 10%, which run over all the possible magnetic configurations in the 30-atom cell and covered the possible magnetic interactions up to next nearest couplings. In fact, all the atomic moments of the spin up and down do not favor AFM after relaxation, with the local atomic moments different in the two spin channels like 3.036 μ_B, -2.392 μ_B, *etc.* This gives rise to a total magnetic moment of about 4 μ_B/cell and the DOS no longer looks like the AFM configurations, which suppose to be symmetrical for spin up and down channels. Meanwhile, as shown in Fig. 6(f), the FM configuration is not the most energetic favorable after reaching the critical points. Thus, the ferrimagnetic behavior is confirmed within the 30-atom cell. In a larger supercell, the new magnetic configurations will involve changes of less nearest and next nearest interactions, and the favored magnetic ferrimagnetic configuration is unlikely to change. Although such large compression may be quite difficult to realize in experiments since such perovskites are easy to be broken down under high pressure [74], the fact that their magnetic exchange energy as well as the ferromagnetism would be sharply weaken is confirmed in our computations. We have carefully checked the energy of these strain states and find that the fitting lines obey the Murganan rule [68] very well as shown in Fig. 6(f).

Last but not the least, we have also investigated the hole doping states of $La_{\frac{2}{3}}Sr_{\frac{1}{3}}MnO_3$ for comparison. Unlike the $La_{\frac{2}{3}}Ca_{\frac{1}{3}}MnO_3$ case, $La_{\frac{2}{3}}Sr_{\frac{1}{3}}MnO_3$ undergoes a phase transition from an FM-metallic state to an FerriM-metallic state when charge doped 0.4 hole/f.u. as Fig. 6 (e)(f) shown. Although such high doping concentration may not easy to realize in experiments, the remarkably weaken ferromagnetism in such situation is confirmed.

4. Conclusion

We have primarily investigated the electronic and magnetic properties of $La_{\frac{2}{3}}M_{\frac{1}{3}}MnO_3$ (M=Ca, Sr) membranes under strain and charge doping conditions based on SCAN+U simulations. For $La_{\frac{2}{3}}Ca_{\frac{1}{3}}MnO_3$, a phase transition from FM-metallic ground state to A-AFM semiconductor ground state is observed under both biaxial and compressive *c*-axis strain conditions in our calculation. We also discover that the trend of variation of magnetic behavior under charge doping is in analogy to the case directly changing the Ca concentrations. It further implies the carrier concentration combined with strains determine the magnetic ground state while the La/Ca distributions have little impact. As for $La_{\frac{2}{3}}Sr_{\frac{1}{3}}MnO_3$, we predict that it could enter into a ferromagnetic-semiconductor ground state under biaxial strain. Furthermore, the energy gap and the magnetic anisotropic energy is remarkably enlarged as strain applies. Under compressive strain, $La_{\frac{2}{3}}Sr_{\frac{1}{3}}MnO_3$ transits into an FerriM-semiconductor ground state. In the hole doping situation, this material will rush into FerriM-metallic ground state when the hole doping concentration reaches 0.4 hole/f.u. We not only offers a comprehensive theoretical understanding of the tunable magnetic and electronic properties of this series but also, hopefully, offer great opportunities for the materials prediction and design in a large number of complex magnetic oxides wherever competing orders exist, such as $La_{1-x}Sr_xCoO_3$ [75], $La_{1-x}Ba_xMnO_3$ [76], $La_{1-x}Sr_xMn_{1-y}Fe_yO_3$ [77], $La(Cr_{0.2}Mn_{0.2}Fe_{0.2}Co_{0.2}Ni_{0.2})O_3$ films [78], $La_{1-x}Na_xMnO_z$ [79], and so on.

CRediT authorship contribution statement

Jia-Yi Lin: Visualization, Writing – original draft, Validation, Conceptualization, Data curation, Formal analysis, Investigation.

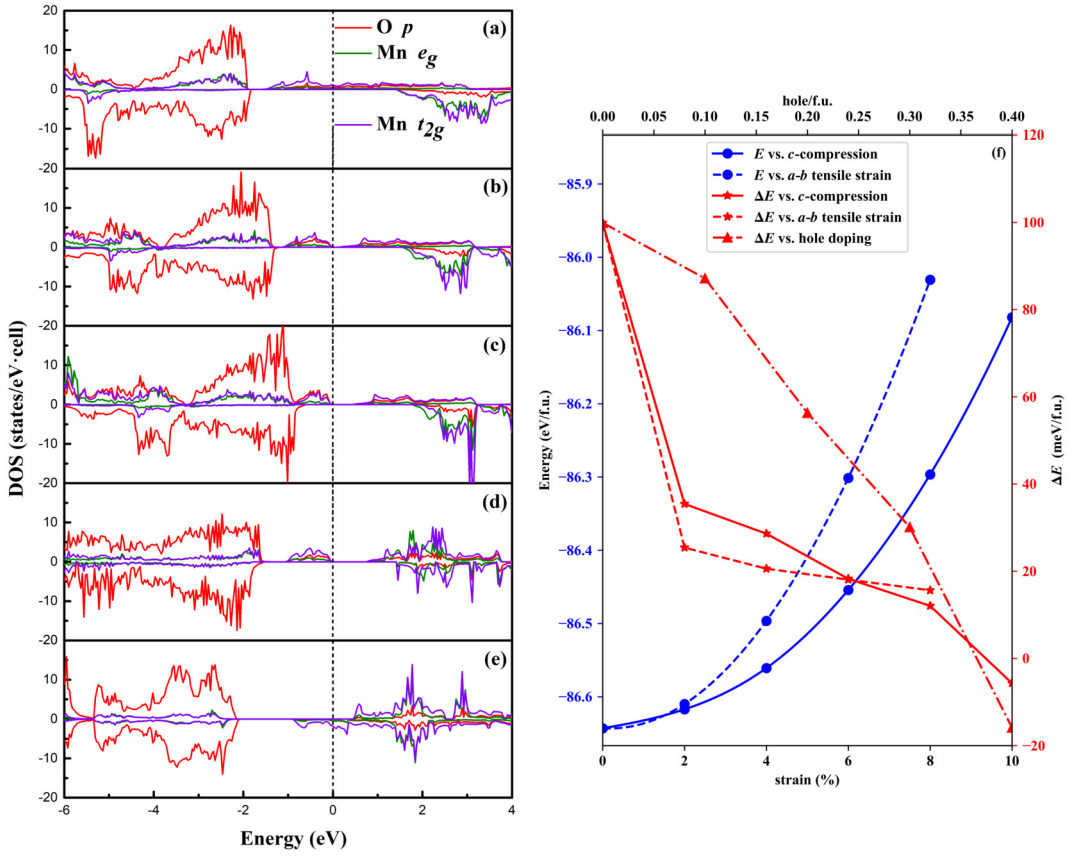

Fig. 6. $La_{\frac{2}{3}}Sr_{\frac{1}{3}}MnO_3$. (a) The PDOS of $La_{\frac{2}{3}}Sr_{\frac{1}{3}}MnO_3$ without strain. (b) The PDOS of biaxial strain 4% state. (c) The PDOS of biaxial strain 8% state. (d) The PDOS of compressive strain 10% state along *c* axis. (e) The PDOS of charge doped 0.4 hole/f.u state. (f) E_{AFM}-E_{FM} vs. biaxial strain; E_{FerriM}-E_{FM} for compressive strain states along *c* axis; E_{FerriM}-E_{FM} vs. hole doping; the total energy for biaxial strain states; the total energy for compressive strain states along *c* axis.

Zhong-Jia Chen: Software, Methodology. **Guan-Liang Li:** Visualization, Writing – review & editing. **Jiarui Zeng:** Writing – review & editing, Software. **Yu-Jie Cen:** Software. **Wen-Qiang Xie:** Visualization. **Yin-Hui Peng:** Visualization. **Ji-Hai Liao:** Conceptualization. **Xiao-Bao Yang:** Supervision. **Yu-Jun Zhao:** Writing – review & editing, Supervision, Software, Resources, Project administration.

Declaration of competing interest

The authors declare that they have no known competing financial interests or personal relationships that could have appeared to influence the work reported in this paper.

Data availability statement

All data presented in this paper are available upon reasonable request.

Acknowledgements

This work is financially supported by NSFC (Grant No. 12074126), the Foundation for Innovative Research Groups of the National Natural Science Foundation of China (Grant No. 51621001), the Fundamental Research Funds for the Central Universities (Grant No. 2020ZYGXZR076), the Guangdong Basic and Applied Basic Research Foundation (No. 2021A1515010349) and the Guangzhou Basic and Applied Basic Research Foundation (No. 202102080166).

References

[1] G.H. Jonker, J.H. Van Santen, Ferromagnetic compounds of manganese with perovskite structure, Physica 16 (1950) 337–349.
[2] M.-H. Phan, S.-C. Yu, Review of the magnetocaloric effect in manganite materials, J. Magn. Magn. Mater. 308 (2007) 325–340.
[3] M.K. Wu, J.R. Ashburn, C.J. Torng, P.H. Hor, R.L. Meng, L. Gao, Z.J. Huang, Y.Q. Wang, C.W. Chu, Superconductivity at 93 K in a new mixed-phase Y-Ba-Cu-O compound system at ambient pressure, Phys. Rev. Lett. 58 (1987) 908–910.
[4] B.S.H. Pang, C. Bell, R.I. Tomov, J.H. Durrell, M.G. Blamire, Pseudo spin-valve behavior in oxide ferromagnet/superconductor/ferromagnet trilayers, Phys. Lett. A 341 (2005) 313–319.
[5] A.P. Ramirez, Colossal magnetoresistance, J. Phys. Condens. Matter 9 (1997) 8171.
[6] J.B. Goodenough, Electronic structure of CMR manganites (invited), J. Appl. Phys. 81 (1997) 5330–5335.
[7] E.L. Nagaev, On the giant magnetoresistance for degenerate ferromagnetic semiconductors of $LaMnO_3$-type, Phys. Lett. A 211 (1996) 313–317.
[8] Y. Tokura, Critical features of colossal magnetoresistive manganites, Rep. Prog. Phys. 69 (2006) 797.
[9] P. Schiffer, A.P. Ramirez, W. Bao, S.-W. Cheong, Low temperature magnetoresistance and the magnetic phase diagram of $La_{1-x}Ca_xMnO_3$, Phys. Rev. Lett. 75 (1995) 3336–3339.
[10] R. Rao, Y.Y. Han, X.C. Kan, X. Zhang, M. Wang, N.X. Qian, G.H. Zheng, Y.Q. Ma, Magnetic property under the pressure and electrical transport behavior under the magnetic field for the perovskite manganite $La_{0.7}Ca_{0.3}MnO_3$, J. Alloys Compd. 837 (2020) 155476.
[11] X. Zhang, Y.Y. Han, X.C. Kan, M. Wang, R. Rao, G.H. Zheng, Y.Q. Ma, Magnetic properties of $La_{0.7}Sr_{0.3}MnO_3$ under the pressure and the transport property under the magnetic field, J. Am. Ceram. Soc. 104 (2021) 955–965.
[12] S. Mori, C.H. Chen, S.-W. Cheong, Pairing of charge-ordered stripes in (La, Ca)MnO_3, Nature 392 (1998) 473–476.
[13] Z.B. Guo, Y.W. Du, J.S. Zhu, H. Huang, W.P. Ding, D. Feng, Large magnetic entropy change in perovskite-type manganese oxides, Phys. Rev. Lett. 78 (1997) 1142–1145.

[14] K. Raju, N.P. Kumar, P.V. Reddy, D.H. Yoon, Influence of Eu doping on magnetocaloric behavior of $La_{0.67}Sr_{0.33}MnO_3$, Phys. Lett. A 379 (2015) 1178–1182.

[15] A. Gómez, E. Chavarriaga, I. Supelano, C.A. Parra, O. Morán, Tuning the magnetocaloric properties of $La_{0.7}Ca_{0.3}MnO_3$ manganites through Ni-doping, Phys. Lett. A 382 (2018) 911–919.

[16] R.H. Yuan, P. Lu, H. Han, D.Z. Xue, A.P. Chen, Q.X. Jia, T. Lookman, Enhanced magnetocaloric performance in manganite bilayers, J. Appl. Phys. 127 (2020) 154102.

[17] Y.L. Zhang, J. Liu, Y.Q. Dong, S.Z. Wu, J.Y. Zhang, J. Wang, J.D. Lu, A. Rückriegel, H.C. Wang, R. Duine, H.M. Yu, Z.L. Luo, K. Shen, J.X. Zhang, Strain-driven Dzyaloshinskii-Moriya interaction for room-temperature magnetic skyrmions, Phys. Rev. Lett. 127 (2021) 117204.

[18] M.S. Ivanov, A.M. Buryakov, P.M. Vilarinho, E.D. Mishina, Impact of compressive and tensile epitaxial strain on transport and nonlinear optical properties of magnetoelectric $BaTiO_3$-(LaCa)MnO_3 tunnel junction, J. Phys. D, Appl. Phys. 54 (2021) 275302.

[19] J.Y. Zhu, Y. Chen, W.F. Xu, J. Yang, W. Bai, G.S. Wang, C.G. Duan, Z. Tang, X.D. Tang, Low-temperature transport properties of chemical solution deposited polycrystalline $La_{0.7}Sr_{0.3}MnO_3$ ferromagnetic films under a magnetic field, Phys. Lett. A 375 (2011) 3103–3106.

[20] X. Chen, B.H. Wang, Y. Chen, H.M. Wei, B.Q. Cao, Tuning Jahn–Teller distortion and electron localization of $LaMnO_3$ epitaxial films via substrate temperature, J. Phys. D, Appl. Phys. 54 (2021) 235302.

[21] L. Li, Y.Y. Ji, Z.Y. Diao, J.D. Zhang, Z.L. Liao, Toward ultrathin ferromagnetic metal of (110) $La_{2/3}Sr_{1/3}MnO_3$ thin films, Appl. Phys. Lett. 117 (2020) 122404.

[22] A. Jayaraman, Diamond anvil cell and high-pressure physical investigations, Rev. Mod. Phys. 55 (1983) 65–108.

[23] S.S. Hong, M.Q. Gu, M. Verma, V. Harbola, B.Y. Wang, D. Lu, A. Vailionis, Y. Hikita, R. Pentcheva, J.M. Rondinelli, et al., Extreme tensile strain states in $La_{0.7}Ca_{0.3}MnO_3$ membranes, Science 368 (2020) 71–76.

[24] A.S. McLeod, J.D. Zhang, M.Q. Gu, F. Jin, G. Zhang, K.W. Post, X.G. Zhao, A.J. Millis, W.B. Wu, J.M. Rondinelli, et al., Multi-messenger nanoprobes of hidden magnetism in a strained manganite, Nat. Mater. 19 (2020) 397–404.

[25] H.B. Wang, F.R. Fan, S.S. Zhu, H. Wu, Doping enhanced ferromagnetism and induced half-metallicity in CrI_3 monolayer, Europhys. Lett. 114 (2016) 47001.

[26] W.-Q. Xie, Z.-W. Lu, C.-C. He, X.-B. Yang, Y.-J. Zhao, Theoretical study of tunable magnetism of two-dimensional $MnSe_2$ through strain, charge, and defect, J. Phys. Condens. Matter 33 (2021) 215803.

[27] C. Tan, W.-Q. Xie, G.L. Zheng, N. Aloufi, S. Albarakati, M. Algarni, J.B. Li, J. Partridge, D. Culcer, X.L. Wang, et al., Gate-controlled magnetic phase transition in a van der Waals magnet Fe_5GeTe_2, Nano Lett. 21 (2021) 5599–5605.

[28] G.L. Zheng, W.-Q. Xie, S. Albarakati, M. Algarni, C. Tan, Y.H. Wang, J.Y. Peng, J. Partridge, L. Farrar, J.B. Yi, Y.M. Xiong, M.L. Tian, Y.-J. Zhao, L. Wang, Gate-tuned interlayer coupling in van der Waals ferromagnet Fe_3GeTe_2 nanoflakes, Phys. Rev. Lett. 125 (2020) 047202.

[29] C. Zener, Interaction between the d-shells in the transition metals. II. Ferromagnetic compounds of manganese with perovskite structure, Phys. Rev. 82 (1951) 403–405.

[30] C. Zener, Interaction between the d shells in the transition metals, Phys. Rev. 81 (1951) 440–444.

[31] S. Yahyaoui, H.T. Diep, Magnetic properties of $(La_{0.56}Ce_{0.14})Sr_{0.30}MnO_3$ perovskite, Phys. Lett. A 380 (2016) 3212–3216.

[32] S. Jin, T.H. Tiefel, M. McCormack, R.A. Fastnacht, R. Ramesh, L.H. Chen, Thousandfold change in resistivity in magnetoresistive La-Ca-Mn-O films, Science 264 (1994) 413–415.

[33] A.J. Millis, P.B. Littlewood, B.I. Shraiman, Double exchange alone does not explain the resistivity of $La_{1-x}Sr_xMnO_3$, Phys. Rev. Lett. 74 (1995) 5144–5147.

[34] W.E. Pickett, D.J. Singh, Electronic structure and half-metallic transport in the $La_{1-x}Ca_xMnO_3$ system, Phys. Rev. B 53 (1996) 1146–1160.

[35] E.A. Kotomin, R.A. Evarestov, Y.A. Mastrikov, J. Maier, DFT plane wave calculations of the atomic and electronic structure of $LaMnO_3$ (001) surface, Phys. Chem. Chem. Phys. 7 (2005) 2346–2350.

[36] T. Hashimoto, S. Ishibashi, K. Terakura, Jahn-Teller distortion and magnetic structure in $LaMnO_3$: a first-principles theoretical study with full structure optimizations, Phys. Rev. B 82 (2010) 045124.

[37] Y.-S. Su, T.A. Kaplan, S.D. Mahanti, J.F. Harrison, Electronic structure of $LaMnO_3$ in the ab initio crystal Hartree-Fock approximation, Phys. Rev. B 61 (2000) 1324–1329.

[38] M. Nicastro, C.H. Patterson, Exchange coupling in $CaMnO_3$ and $LaMnO_3$: configuration interaction and the coupling mechanism, Phys. Rev. B 65 (2002) 205111.

[39] D. Muñoz, N.M. Harrison, F. Illas, Electronic and magnetic structure of $LaMnO_3$ from hybrid periodic density-functional theory, Phys. Rev. B 69 (2004) 085115.

[40] A.D. Becke, A new mixing of Hartree-Fock and local density-functional theories, J. Chem. Phys. 98 (1993) 1372–1377.

[41] J.P. Perdew, M. Ernzerhof, K. Burke, Rationale for mixing exact exchange with density functional approximations, J. Chem. Phys. 105 (1996) 9982–9985.

[42] G. Trimarchi, N. Binggeli, Structural and electronic properties of $LaMnO_3$ under pressure: an ab initio LDA + U study, Phys. Rev. B 71 (2005) 035101.

[43] M.T. Christophe Audouze, François Jollet, X. Gonze, Comparison between projector augmented-wave and ultrasoft pseudopotential formalisms at the density-functional perturbation theory level, Phys. Rev. B 78 (2008) 035105.

[44] R. Korotana, G. Mallia, Z. Gercsi, L. Liborio, N.M. Harrison, Hybrid density functional study of structural, bonding, and electronic properties of the manganite series $La_{1-x}Ca_xMnO_3$ ($x = 0, \frac{1}{4}, 1$), Phys. Rev. B 89 (2014) 205110.

[45] R. Korotana, G. Mallia, Z. Gercsi, N.M. Harrison, A hybrid-exchange density functional study of Ca-doped $LaMnO_3$, J. Appl. Phys. 113 (2013) 17A910.

[46] W.D. Luo, S.J. Pennycook, S.T. Pantelides, Magnetic "dead" layer at a complex oxide interface, Phys. Rev. Lett. 101 (2008) 247204.

[47] H. Hmok, E. Martínez-Aguilar, J. Ribas-Ariño, J.M.S. Beltrones, J.L.S. Llamazares, O.R. Herrera, Effect of La^{3+}/Sr^{2+} ordering on the magnetic properties of $La_{2/3}Sr_{1/3}MnO_3$ by first principles calculations, Comput. Mater. Sci. 177 (2020) 109575.

[48] J. Jiang, Q.-M. Chen, X. Liu, First-principles study on the electronic structure and optical properties of $La_{0.75}Sr_{0.25}MnO_3$-σ materials with oxygen vacancies defects, Curr. Appl. Phys. 18 (2018) 200–208.

[49] S. Gong, B.-G. Liu, Electronic energy gaps and optical properties of $LaMnO_3$, Phys. Lett. A 375 (2011) 1477–1480.

[50] S.S. Subramanian, S. Anandan, B. Natesan, Stabilization of E-type antiferromagnetic ordering in La and Y substituted orthorhombic $LuMnO_3$: a first-principles study, Phys. Lett. A 383 (2019) 125950.

[51] J.W. Sun, A. Ruzsinszky, J.P. Perdew, Strongly constrained and appropriately normed semilocal density functional, Phys. Rev. Lett. 115 (2015) 036402.

[52] A.I. Liechtenstein, V.I. Anisimov, J. Zaanen, Density-functional theory and strong interactions: orbital ordering in Mott-Hubbard insulators, Phys. Rev. B 52 (1995) R5467–R5470.

[53] J.W. Sun, R.C. Remsing, Y.B. Zhang, Z.R. Sun, A. Ruzsinszky, H.W. Peng, Z.H. Yang, A. Paul, U. Waghmare, X.F. Wu, et al., Accurate first-principles structures and energies of diversely bonded systems from an efficient density functional, Nat. Chem. 8 (2016) 831–836.

[54] G. Kresse, D. Joubert, From ultrasoft pseudopotentials to the projector augmented-wave method, Phys. Rev. B 59 (1999) 1758–1775.

[55] G. Kresse, J. Furthmüller, Efficiency of ab-initio total energy calculations for metals and semiconductors using a plane-wave basis set, Comput. Mater. Sci. 6 (1996) 15–50.

[56] G. Kresse, J. Hafner, Ab initio molecular dynamics for open-shell transition metals, Phys. Rev. B 48 (1993) 13115–13118.

[57] G. Kresse, J. Hafner, Ab initio molecular dynamics for liquid metals, Phys. Rev. B 47 (1993) 558–561.

[58] G. Kresse, J. Furthmüller, Efficient iterative schemes for ab initio total-energy calculations using a plane-wave basis set, Phys. Rev. B 54 (1996) 11169–11186.

[59] P.E. Blöchl, Projector augmented-wave method, Phys. Rev. B 50 (1994) 17953–17979.

[60] C.-C. He, S.-B. Qiu, J.-S. Yu, J.-H. Liao, Y.-J. Zhao, X.-B. Yang, Atom classification model for total energy evaluation of two-dimensional multicomponent materials, J. Phys. Chem. A 124 (2020) 4506–4511.

[61] C.-C. He, J.-H. Liao, S.-B. Qiu, Y.-J. Zhao, X.-B. Yang, Biased screening for multicomponent materials with structures of Alloy Generation and Recognition (SAGAR), Comput. Mater. Sci. 193 (2021) 110386.

[62] V. Wang, N. Xu, J.-C. Liu, G. Tang, W.-T. Geng, VASPKIT: a user-friendly interface facilitating high-throughput computing and analysis using VASP code, Comput. Phys. Commun. (2021) 108033.

[63] W.J. Lu, Y.P. Sun, X.B. Zhu, W.H. Song, J.J. Du, Destabilization of the cooperative Jahn-Teller effect in $Sr_{0.9}Ce_{0.1}MnO_3$ by Cr-doping, Phys. Lett. A 349 (2006) 388–392.

[64] E. Restrepo-Parra, C.D. Salazar-Enríquez, J. Londoño-Navarro, J.F. Jurado, J. Restrepo, Magnetic phase diagram simulation of $La_{1-x}Ca_xMnO_3$ system by using Monte Carlo, Metropolis algorithm and Heisenberg model, J. Magn. Magn. Mater. 323 (2011) 1477–1483.

[65] H. Tsukahara, S. Ishibashi, K. Terakura, First-principles calculations for the magnetic phase diagram in electron-doped $CaMnO_3$ under compressive and tensile strains, Phys. Rev. B 81 (2010) 214108.

[66] E.O. Wollan, W.C. Koehler, Neutron diffraction study of the magnetic properties of the series of perovskite-type compounds $[(1-x)La, xCa]MnO_3$, Phys. Rev. 100 (1955) 545–563.

[67] Y.H. Liu, L.-L. Wang, Q. Zheng, Z.L. Huang, X.P. Wang, M.F. Chi, Y. Wu, B.C. Chakoumakos, M.A. McGuire, B.C. Sales, W.D. Wu, J.Q. Yan, Site mixing for engineering magnetic topological insulators, Phys. Rev. X 11 (2021) 021033.

[68] P. Vinet, J.H. Rose, J. Ferrante, J.R. Smith, Universal features of the equation of state of solids, J. Phys. Condens. Matter 1 (1989) 1941.

[69] M. Ziese, I. Vrejoiu, E. Pippel, P. Esquinazi, D. Hesse, C. Etz, J. Henk, A. Ernst, I.V. Maznichenko, W. Hergert, I. Mertig, Tailoring magnetic interlayer coupling in $La_{0.7}Sr_{0.3}MnO_3/SrRuO_3$ superlattices, Phys. Rev. Lett. 104 (2010) 167203.

[70] P.X. Zhou, J.M. Wang, H.C. Liu, L.C. Zhao, Q. Yang, C.G. Zhong, Z.Y. Zhao, L.H. Qu, Z.C. Dong, Emergent multiferroicity and strain-driven metal-semiconductor transitions in $LaMnO_3/RMnO_3$ superlattices (R = Pr, Pm, Sm and Gd), Phys. Chem. Chem. Phys. 22 (2020) 17503–17512.

[71] L.-D. Yuan, Z. Wang, J.-W. Luo, A. Zunger, Prediction of low-Z collinear and noncollinear antiferromagnetic compounds having momentum-dependent spin splitting even without spin-orbit coupling, Phys. Rev. Mater. 5 (2021) 014409.

[72] S.V. Halilov, A.Y. Perlov, P.M. Oppeneer, A.N. Yaresko, V.N. Antonov, Magnetocrystalline anisotropy energy in cubic Fe, Co, and Ni: applicability of local-spin-density theory reexamined, Phys. Rev. B 57 (1998) 9557–9560.
[73] Z.-Z. Lin, X. Chen, 1T GdN_2 monolayer—spin-orbit induced magnetic Dirac semiconductor stable at room temperature, Appl. Surf. Sci. 529 (2020) 147129.
[74] D.P. Kozlenko, N.T. Dang, S.E. Kichanov, E.V. Lukin, K. Knizek, Z. Jirák, L.S. Dubrovinsky, V.I. Voronin, B.N. Savenko, Pressure-induced structural transformations, orbital order and antiferromagnetism in $La_{0.75}Ca_{0.25}MnO_3$, Eur. Phys. J. B 86 (2013) 1–8.
[75] W. Wang, J. Zhang, X. Shen, X.X. Guan, Y. Yao, J.J. Li, C.Z. Gu, J.R. Sun, Y.M. Zhu, J. Tao, R.C. Yu, Out-of-plane magnetic anisotropy enhancement in $La_{1-x}Sr_xCoO_{3-\delta}/La_{2/3}Sr_{1/3}MnO_3/La_{1-x}Sr_xCoO_{3-\delta}$ thin films, Phys. Rev. B 101 (2020) 024406.
[76] N.G. Bebenin, N.N. Loshkareva, A.A. Makhnev, E.V. Mostovshchikova, L.V. Nomerovannaya, E.A. Gan'shina, A.N. Vinogradov, Y.M. Mukovskii, Optical and magneto-optical properties of ferromagnetic $La_{1-x}Ba_xMnO_3$ single crystals, J. Phys. Condens. Matter 22 (2010) 096003.
[77] V.S. Zakhvalinskii, R. Laiho, A.V. Lashkul, K.G. Lisunov, E. Lähderanta, Y.S. Nekrasova, P.A. Petrenko, V.N. Stamov, Variable-range hopping conductivity of $La_{1-x}Sr_xMn_{1-y}Fe_yO_3$, J. Phys. Condens. Matter 23 (2010) 015802.
[78] M. Brahlek, A.R. Mazza, K.C. Pitike, E. Skoropata, J. Lapano, G. Eres, V.R. Cooper, T.Z. Ward, Unexpected crystalline homogeneity from the disordered bond network in $La(Cr_{0.2}Mn_{0.2}Fe_{0.2}Co_{0.2}Ni_{0.2})O_3$ films, Phys. Rev. Mater. 4 (2020) 054407.
[79] Z.Q. Li, E.Y. Jiang, D.X. Zhang, D.L. Hou, W.C. Li, H.L. Bai, Effect of annealing on polycrystalline $La_{1-x}Na_xMnO_z$ ceramics, Phys. Lett. A 277 (2000) 56–60.